
Electronic Supplementary Information

Computational Kinetics of the Hydrogen Abstraction Reactions of *n*-propanol and *iso*-propanol by OH Radical

Xuan Guo,^{1,2} Rui Ming Zhang,¹ Lu Gem Gao,¹ Xin Zhang,^{2,*} and Xuefei Xu^{1,*}

¹Center for Combustion Energy, Department of Energy and Power Engineering, and Key Laboratory for Thermal Science and Power Engineering of Ministry of Education, Tsinghua University, Beijing 100084, China

²State Key Laboratory of Chemical Resource Engineering, Beijing Advanced Innovation Center for Soft Matter Science and Engineering, Beijing University of Chemical Technology, Beijing 100029, P. R. China

Contents

Section 1. Additional Computational Details	S-3
Section 2. F_{act}^{MS-T} and $F^{MS-T,\alpha}$	S-3
Section 3. Specific-Reaction-Parameter (SRP) Scaling Factor of Frequencies	S-4
Section 4. Transmission Coefficients	S-5
Table S1. T_1 Diagnostic Values	S-7
Table S2. Forward and Reverse Barrier Heights, Energies of Reaction, and Mean Unsigned Deviations from Best Estimates (in kcal/mol) for <i>n</i> -Propanol	S-7
Table S3. Forward and Reverse Barrier Heights, Energies of Reaction, and Mean Unsigned Deviations from Best Estimates (in kcal/mol) for <i>i</i> -Propanol	S-8
Table S4. Zero-Point Energies (in kcal/mol) and SRP Scaling Factors for TS and Pre-reactive Complex for <i>n</i> -Propanol	S-8
Table S5. Zero-Point Energies (in kcal/mol) and SRP Scaling Factors for TS and Pre-reactive Complex for <i>i</i> -Propanol	S-9
Table S6. The CCUS rate Constants (in $\text{cm}^3\text{molecule}^{-1}\text{s}^{-1}$) Calculated Using the Standard Scaling Factor or SRP Factors of <i>n</i> -Propanol.	S-9
Table S7. The CCUS rate Constants (in $\text{cm}^3\text{molecule}^{-1}\text{s}^{-1}$) Calculated Using the Standard Scaling Factor or SRP Factors of <i>i</i> -Propanol.	S-10

Figure S1. Lowest-Energy Structures of Reactants, Complex, Transition States and Products for <i>n</i> -Propanol Reactions with OH	S-11
Figure S2. Lowest-Energy Structures of Reactants, Complex, Transition States and Products for <i>i</i> -Propanol Reactions with OH	S-12
Figure S3. Multi-Structural Anharmonicity Factors $F^{\text{MS-T},\alpha}$ for (a) <i>n</i> -Propanol and Four Transition States. (b) <i>i</i> -Propanol and Three Transition States.	S-12
Figure S4. The Number of Conformations of the Transition States for <i>n</i> -Propanol (a) and <i>i</i> -Propanol (b) Reactions and the Energy Relative to the Lowest -Energy Conformation (in kcal/mol)	S-13
Figure S5. Calculated Ground-State Vibrationally Adiabatic Potential Curves (V_a^G) of Reactions R1 and R2 as Functions of the Reaction Coordinates s .	S-13
References	S-13

1. Additional Computational Details

In the CCUS method, we use the hard-sphere collision rate constant formula to estimate the capture rate constant k_a :

$$k_a = \pi \left(\frac{d_{OH} + d_{ROH}}{2} \right)^2 \sqrt{\frac{8k_B T}{\pi \mu}} \quad (1)$$

where we use ROH to represent *n*-propanol or *i*-propanol, and μ is the reduced mass of OH and ROH, and d_{OH} and d_{ROH} are van der Waals diameters of OH and ROH.

The T_1 diagnostics were calculated with the CCSD/jul-cc-pVTZ method and given in Table S1. The geometries used in T_1 calculations were the lowest-energy structures obtained at the M08-HX/MG3S level (see Figure S1 and S2), which can give accurate geometries for transition states.

2. F_{act}^{MS-T} and $F^{MS-T,\alpha}$

The multi-structural torsional anharmonicity factor F_{act}^{MS-T} of the particular reaction rate is calculated as the ratio of multi-structural torsional factors $F^{MS-T,\alpha}$ of the transition state ($\alpha=TSb,j$) and reactant ($\alpha=R$):

$$F_{act}^{MS-T} = \frac{F^{MS-T,TSb,j}}{F^{MS-T,R}} \quad (2)$$

where the multi-structural torsional factor $F^{MS-T,\alpha}$ of species α is obtained by:

$$F^{MS-T,\alpha} = \frac{Q_{con-rovib}^{MS-T,\alpha}}{Q_{rovib,1}^{SS-HO,\alpha}} \quad (3)$$

in which $Q_{rovib,1}^{SS-HO,\alpha}$ is the rotational-vibrational partition function of the lowest-potential-energy structure 1 of the species α calculated in the single-structure harmonic approximation, and $Q_{con-rovib}^{MS-T,\alpha}$ is the conformational-rotational-vibrational partition function of the species α calculated by the multi-structural torsional method with a coupled torsional potential. The latter considers both the multiple structural effect from all the distinguishable conformers of the interested species and the effect of torsional anharmonicity.

After a detailed multi-structure search, the located lowest-energy structures of species by the M08-HX/MG3S method are displayed in Figures S1 and S2.

Figure S3 shows the reactant *n*-propanol has a similar MS-T anharmonicity to those of the transition states of reactions at low temperatures but much smaller MS-T anharmonicity at high temperatures because it has less torsional degrees of freedom and

correspondingly less distinguishable conformational structures than those transition states.

Although the H_O-abstraction (R1d) transition state of *n*-propanol has much less conformers than the transition states of H_α and H_β abstractions (R1a and R1b), since it has more low-energy structures with energies difference within 1.5 kcal/mol (see Figure S4a), it has a larger MS-T anharmonicity Factor at $T > \sim 340$ K than the other channels' transition structures. For *i*-propanol reactions, the H_γ-abstraction transition state has remarkably larger MS-T factor than the other transition structures of *i*-propanol because it has much more conformers (See Figure S4b).

3. Specific-Reaction-Parameter (SRP) Scaling Factor of Frequencies

The λ^{SRP} scaling factor is obtained by¹:

$$\lambda^{\text{SRP}} = \lambda^{\text{Anh}} \lambda^{\text{H}} \quad (4)$$

where λ^{Anh} is the correction to anharmonicity of the zero point energy (ZPE), and λ^{H} is the correction to inaccuracy of the given model chemistry. We obtain λ^{H} by parametrization to obtain the accurate harmonic frequencies in the F38/10 database¹ as usual.

The λ^{Anh} scaling factor is calculated as

$$\lambda^{\text{Anh}} = \text{ZPE}^{\text{Anh}} / \text{ZPE}^{\text{Harm}} \quad (5)$$

where ZPE^{Anh} and ZPE^{Harm} are anharmonic ZPE and ZPE computed in the harmonic approximation, respectively.

We calculated the specific-reaction-parameter (SRP) scaling factor λ^{SRP} of frequencies for the lowest-energy structures of transition states and the pre-reactive complex by using eqs (4) and (5) and the particularly selected model chemistry for that reaction channel, and these λ^{SRP} factors are listed in Table S4 and S5, as well as the standard scaling factors λ^{STD} for comparison. The calculated λ^{SRP} scaling factors for transition states are much smaller than the standard scaling factors λ^{STD} , and the λ^{SRP} scaling factors of the complexes are close to the corresponding λ^{STD} factors. This agrees with the previous study for OH reactions with methanol or with isobutanol^{2,3}: the unstable transition structures exhibit greater anharmonicity of high-frequency modes than the stable reactant molecules.

4. Transmission Coefficients.

4.1 I^{CVT}

Figure S4 shows the common logarithm of the calculated recrossing transmission coefficients I^{CVT} as functions of $1000/T$, which is an estimate of variational effect and is defined as a ratio of a quasiclassical variational transition-state theory rate constant to a quasiclassical conventional transition-state theory rate constant. Inspection of Figure 5 in the manuscript shows that for both *n*-propanol and *i*-propanol reactions, the H_o-abstraction channel has relatively weaker variational effect than other channels at the same temperature. All channels exhibit monotonic increasing variational effect (decreasing value of I^{CVT}) with decreasing temperature. Remarkable variational effect is observed below 500 K for all the studied reactions channels. Take the H_α-abstraction as example, I^{CVT} is 0.55 for *n*-propanol and 0.38 for *i*-propanol at 500 K, then I^{CVT} is decreased to 0.32 for *n*-propanol and 0.22 for *i*-propanol at 298 K, respectively. At the studied lowest temperature (63 K), the variational effect can reduce the rate constants up to by three orders of magnitude. These features about variation effect were also found in the OH + methanol reactions². Therefore, the variational effect has to be considered for the kinetics study of OH reactions with alcohols in the ultralow temperature regime.

4.2 κ^{SCT}

The κ^{SCT} transmission coefficient is assumed to be the ground-state transmission coefficient with the ground-state vibrationally adiabatic potential energy curve (V_a^{G})⁴ as the effective barrier,

$$V_a^{\text{G}} = V_{\text{MEP}}(s) + \text{ZPE}(s) \quad (6)$$

where $V_{\text{MEP}}(s)$ is the potential energy along the minimum energy path (MEP), s is the signed distance along MEP, and $\text{ZPE}(s)$ denotes the local zero-point vibrational energy of the bound modes transverse to the reaction coordinate at s . Note that we use the quantized-reactant-state tunneling (QRST) approximation⁵ in the SCT tunneling calculations in the high-pressure limit because we are investigating rate constants down

to ultra-low temperatures and considering the tunneling from the low-energy states of the complex.

Figure 6 in the manuscript plots the tunneling transmission coefficient κ^{SCT} calculated in the small curvature approximation in both low-pressure and high-pressure limits. As we expected, considerably large tunneling effects are observed in the low temperature regime, and at ultracold temperatures, the tunneling through the barrier of reaction in the HP limit can be several orders of magnitude greater than that in the LP limit. In both limits, the channel with larger barrier has larger tunneling at the same temperature. The H_o-abstraction channel shows significantly larger tunneling effect than other channels for $T < 250$ K.

Table S1. T_1 Diagnostic Values

	R1a	R1b	R1c	R1d	R2a	R2b	R2c
TS	0.024	0.023	0.023	0.042	0.024	0.024	0.042
Product radical	0.014	0.012	0.011	0.018	0.014	0.012	0.018
<i>n</i> -propanol	0.010						
<i>i</i> -propanol	0.010						
OH	0.009						
H ₂ O	0.009						

Table S2. Forward and Reverse Barrier Heights, Energies of Reaction, and Mean Unsigned Deviations from Best Estimates (in kcal/mol) for *n*-Propanol.

	Functional	V^\ddagger		ΔV	MUD ^a
		Forward	Reverse		
R1a	M08-HX	0.31	0.54	0.85	0.56
	M08-SO	1.37	0.20	1.17	0.91
	M06-2X	0.87	0.88	0.01	0.59
	MN15-L	2.21	2.17	0.04	1.48
	MPW1K	0.99	0.59	1.58	1.05
R1b	M08-HX	0.03	0.61	0.63	0.42
	M08-SO	1.39	0.48	1.87	1.25
	M06-2X	0.79	0.57	0.22	0.53
	MN15-L	0.07	0.98	1.05	0.70
	MPW1K	1.35	0.06	1.29	0.90
R1c	M08-HX	0.02	0.36	0.39	0.26
	M08-SO	1.35	0.22	1.13	0.90
	M06-2X	0.82	0.81	0.00	0.54
	MN15-L	1.09	1.52	0.43	1.02
	MPW1K	1.21	0.82	2.03	1.36
R1d	M08-HX	0.03	1.05	1.02	0.70
	M08-SO	1.72	0.69	1.03	1.15
	M06-2X	2.02	1.37	0.65	1.35
	MN15-L	3.08	1.33	1.75	2.05
	MPW1K	1.38	2.35	0.97	1.57

^aMUD is the mean unsigned deviation of the classical reaction energy and the classical barrier heights from CCSD(T)-F12a/jul-cc-pVTZ//M08-2X/MG3S benchmark results.

Table S3. Forward and Reverse Barrier Heights, Energies of Reaction, and Mean

Unsigned Deviations from Best Estimates (in kcal/mol) for *i*-Propanol.

	Functional	V^\ddagger		ΔV	MUD
		Forward	Reverse		
R2a	M08-HX	0.18	1.32	1.14	0.88
	M08-SO	0.87	0.87	1.74	1.16
	M06-2X	0.47	0.08	0.39	0.31
	MN15-L	1.28	0.09	1.19	0.85
	MPW1K	0.76	0.13	0.64	0.51
R2b	M08-HX	0.35	0.50	0.15	0.33
	M08-SO	0.92	0.17	1.09	0.73
	M06-2X	0.47	0.74	0.27	0.50
	MN15-L	0.27	0.15	0.13	0.18
	MPW1K	1.13	1.03	2.16	1.44
R2c	M08-HX	0.25	0.55	0.81	0.54
	M08-SO	2.00	1.00	0.99	1.33
	M06-2X	2.13	1.57	0.55	1.42
	MN15-L	3.49	2.25	1.24	2.33
	MPW1K	1.71	2.63	0.91	1.75

Table S4. Zero-Point Energies (in kcal/mol) and SRP Scaling Factors for TS and Pre-reactive Complex for *n*-Propanol

	ZPE(Harm)	ZPE(Anh)	λ^{Anh}	λ^{H}	SRP λ^{ZPE}	STD λ^{ZPE}
R1a TS	75.27	73.51	0.977	0.984	0.961	0.973
R1b TS	74.30	72.34	0.974	0.984	0.958	
R1c TS	74.36	72.85	0.980	0.984	0.964	
R1d TS	73.93	72.27	0.978	0.984	0.962	
R1a RC	77.36	76.30	0.986	0.984	0.970	0.973
R1b RC	77.37	76.18	0.985	0.984	0.969	
R1c RC	77.37	76.18	0.985	0.984	0.969	
R1d RC	77.37	76.18	0.985	0.984	0.969	

Table S5. Zero-Point Energies (in kcal/mol) and SRP Scaling Factors for TS and Pre-reactive Complex for *i*-Propanol

	ZPE(Harm)	ZPE(Anh)	λ^{Anh}	λ^{H}	SRP λ^{ZPE}	STD λ^{ZPE}
--	-----------	----------	------------------------	----------------------	----------------------------	----------------------------

R2a TS	75.12	73.78	0.982	0.982	0.965	0.970
R2b TS	73.78	72.25	0.979	0.991	0.970	0.977
R2c TS	73.47	71.77	0.977	0.984	0.961	0.973
R2a RC	76.88	75.69	0.985	0.982	0.967	0.970
R2b RC	76.87	75.68	0.985	0.991	0.976	0.977
R2c RC	76.87	75.68	0.985	0.984	0.969	0.973

Table S6. The CCUS rate Constants (in $\text{cm}^3\text{molecule}^{-1}\text{s}^{-1}$) Calculated Using the Standard Scaling Factor or SRP Factors of *n*-Propanol.

$T(\text{K})$	LPL-CCUS		HPL-CCUS	
	STD	SRP	STD	SRP
63	1.29E-12	1.69E-10	1.86E-10	1.86E-10
73	1.02E-12	1.47E-10	2.00E-10	2.00E-10
80	9.10E-13	1.21E-10	2.09E-10	2.09E-10
87	8.26E-13	9.46E-11	2.18E-10	2.18E-10
93	7.72E-13	7.47E-11	2.26E-10	2.26E-10
100	7.23E-13	5.65E-11	2.33E-10	2.34E-10
110	6.74E-13	3.87E-11	2.29E-10	2.45E-10
120	6.37E-13	2.76E-11	1.77E-10	2.52E-10
130	6.14E-13	2.05E-11	8.81E-11	2.49E-10
140	5.97E-13	1.58E-11	3.81E-11	2.22E-10
150	5.85E-13	1.27E-11	1.81E-11	1.74E-10
160	5.78E-13	1.04E-11	1.03E-11	1.24E-10
170	5.74E-13	8.84E-12	6.63E-12	8.47E-11
180	5.74E-13	7.65E-12	4.74E-12	5.87E-11
190	5.76E-13	6.73E-12	3.65E-12	4.20E-11
200	5.80E-13	6.02E-12	2.97E-12	3.13E-11
220	5.93E-13	5.02E-12	2.20E-12	1.94E-11
240	6.12E-13	4.38E-12	1.80E-12	1.35E-11
260	6.37E-13	3.94E-12	1.58E-12	1.02E-11
280	6.66E-13	3.65E-12	1.45E-12	8.30E-12
298.15	6.96E-13	3.46E-12	1.38E-12	7.13E-12
320	7.38E-13	3.30E-12	1.33E-12	6.19E-12
340	7.80E-13	3.22E-12	1.31E-12	5.62E-12
360	8.26E-13	3.18E-12	1.31E-12	5.24E-12
380	8.75E-13	3.16E-12	1.32E-12	4.95E-12
400	9.27E-13	3.16E-12	1.35E-12	4.74E-12
435	1.03E-12	3.21E-12	1.41E-12	4.53E-12
470	1.14E-12	3.31E-12	1.50E-12	4.47E-12
500	1.25E-12	3.43E-12	1.58E-12	4.47E-12
550	1.45E-12	3.69E-12	1.76E-12	4.61E-12
600	1.67E-12	4.01E-12	1.97E-12	4.84E-12

700	2.20E-12	4.81E-12	2.47E-12	5.54E-12
800	2.84E-12	5.80E-12	3.08E-12	6.48E-12
900	3.60E-12	6.97E-12	3.03E-12	7.62E-12
1000	4.46E-12	8.35E-12	3.92E-12	8.98E-12
1200	6.50E-12	1.15E-11	6.00E-12	1.21E-11
1400	9.10E-12	1.55E-11	8.59E-12	1.61E-11
1600	1.23E-11	2.04E-11	1.18E-11	2.11E-11
1800	1.61E-11	2.62E-11	1.55E-11	2.68E-11
2000	2.04E-11	3.27E-11	1.97E-11	3.34E-11

Table S7. The CCUS rate Constants (in $\text{cm}^3\text{molecule}^{-1}\text{s}^{-1}$) Calculated Using the Standard Scaling Factor or SRP Factors of *i*-Propanol.

$T(\text{K})$	LPL-CCUS		HPL-CCUS	
	STD	SRP	STD	SRP
63	1.52E-10	1.84E-10	1.86E-10	1.86E-10
73	1.12E-10	1.91E-10	2.00E-10	2.00E-10
80	8.20E-11	1.87E-10	2.08E-10	2.09E-10
87	5.76E-11	1.74E-10	2.09E-10	2.18E-10
93	4.27E-11	1.54E-10	1.93E-10	2.25E-10
100	3.06E-11	1.27E-10	1.54E-10	2.30E-10
110	1.99E-11	9.02E-11	9.21E-11	2.17E-10
120	1.38E-11	6.24E-11	5.30E-11	1.73E-10
130	1.01E-11	4.33E-11	3.22E-11	1.20E-10
140	7.73E-12	3.11E-11	2.10E-11	8.05E-11
150	6.13E-12	2.30E-11	1.46E-11	5.46E-11
160	5.02E-12	1.76E-11	1.07E-11	3.83E-11
170	4.23E-12	1.39E-11	8.27E-12	2.80E-11
180	3.65E-12	1.13E-11	6.61E-12	2.13E-11
190	3.21E-12	9.45E-12	5.46E-12	1.67E-11
200	2.87E-12	8.05E-12	4.62E-12	1.35E-11
220	2.39E-12	6.12E-12	3.54E-12	9.48E-12
240	2.09E-12	4.97E-12	2.90E-12	7.23E-12
260	1.88E-12	4.22E-12	2.48E-12	5.84E-12
280	1.75E-12	3.71E-12	2.22E-12	4.94E-12
298.15	1.66E-12	3.39E-12	2.05E-12	4.38E-12
320	1.59E-12	3.12E-12	1.91E-12	3.91E-12
340	1.56E-12	2.95E-12	1.83E-12	3.62E-12
360	1.55E-12	2.83E-12	1.78E-12	3.41E-12
380	1.54E-12	2.75E-12	1.75E-12	3.27E-12
400	1.56E-12	2.71E-12	1.74E-12	3.17E-12
435	1.60E-12	2.69E-12	1.76E-12	3.09E-12
470	1.68E-12	2.74E-12	1.81E-12	3.08E-12

500	1.75E-12	2.80E-12	1.87E-12	3.13E-12
550	1.92E-12	2.98E-12	2.02E-12	3.27E-12
600	2.12E-12	3.21E-12	2.21E-12	3.48E-12
700	2.61E-12	3.82E-12	2.69E-12	4.07E-12
800	3.26E-12	4.66E-12	3.32E-12	4.90E-12
900	4.08E-12	5.72E-12	4.13E-12	5.94E-12
1000	5.06E-12	7.00E-12	5.10E-12	7.22E-12
1200	7.57E-12	1.03E-11	7.59E-12	1.05E-11
1400	1.09E-11	1.46E-11	1.09E-11	1.48E-11
1600	1.49E-11	1.98E-11	1.49E-11	2.01E-11
1800	1.98E-11	2.62E-11	1.97E-11	2.64E-11
2000	2.55E-11	3.36E-11	2.54E-11	3.39E-11

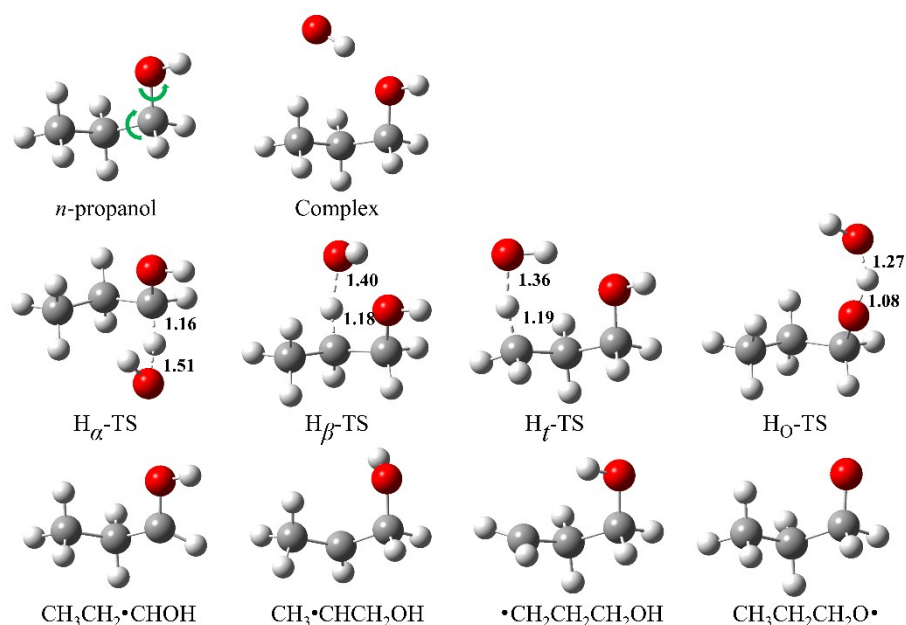


Fig. S1 Lowest-Energy Structures of Reactant, Complex, Transition States and Products for n -Propanol Reactions with OH

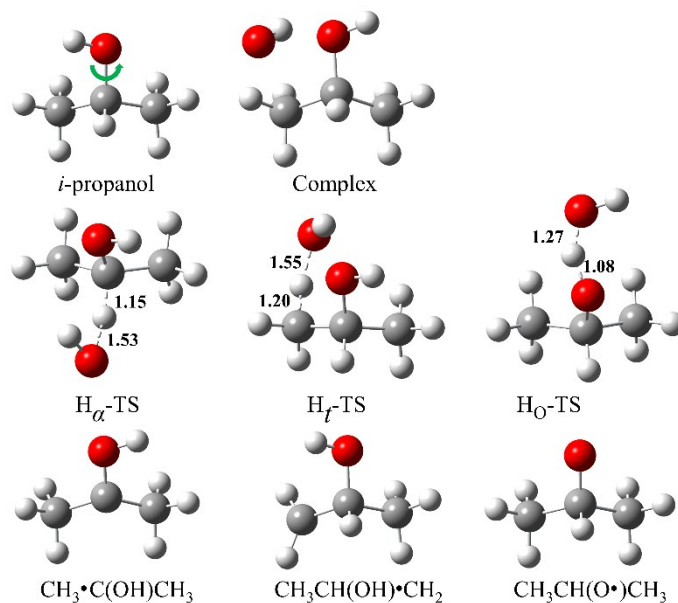


Fig. S2 Lowest-Energy Structures of Reactant, Complex, Transition States and Products for *i*-Propanol Reactions with OH

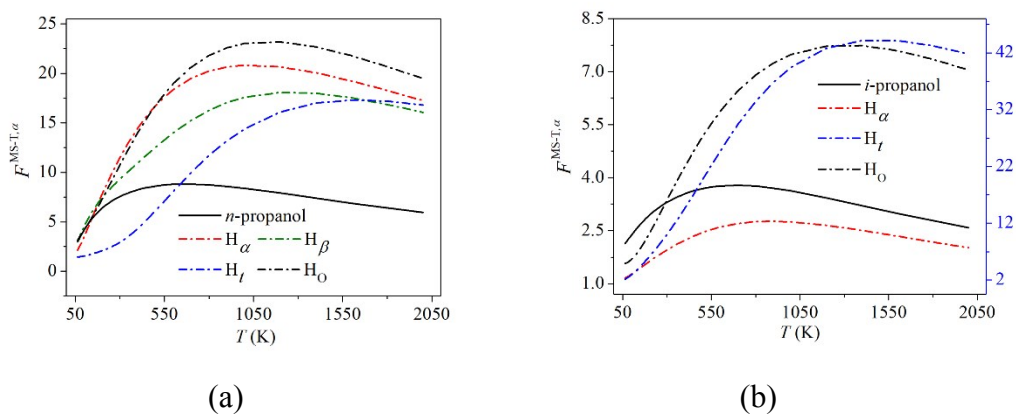


Fig. S3 Multi-Structural Anharmonicity Factors $F^{\text{MS-T},\alpha}$ for (a) *n*-Propanol and Four Transition States. (b) *i*-Propanol and Three Transition States. The Right Ordinate Scale is for the R2b Transition State and the Left Ordinate Scale is for the Remaining Channels, *i*-Propanol, R2a and R2c.

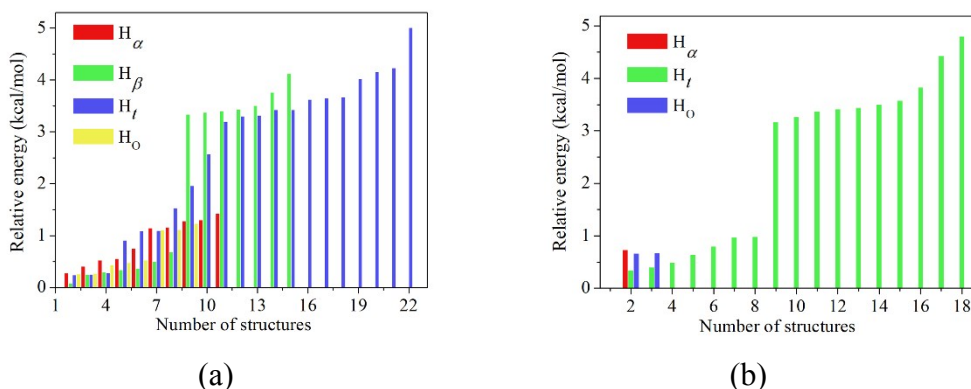


Fig. S4 The Number of Conformations of the Transition States for *n*-Propanol (a) and *i*-Propanol (b) Reactions and the Energy Relative to the Lowest -Energy Conformation (in kcal/mol)

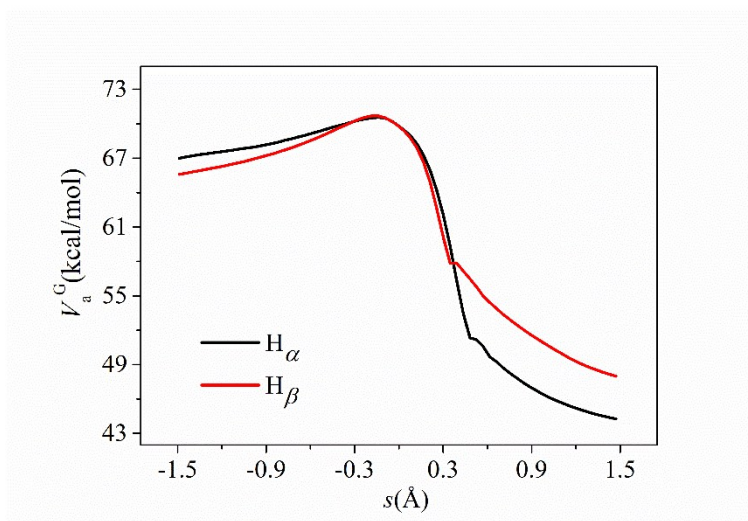


Figure S5. Calculated ground-state vibrationally adiabatic potential curves (V_a^G) of reactions R1a and R1b as functions of the reaction coordinates s , where the reaction coordinates are scaled to a reduced mass of 1 amu.

¹ I.M. Alecu, J. Zheng, Y. Zhao, and D. G. Truhlar. *Journal of Chemical Theory and Computation*, 2010, **6**, 2872-2887.

² L. G. Gao, J. Zheng, A. Fernandez-Ramos, D. G. Truhlar, and X. Xu. *J. Am. Chem. Soc.*, 2018, **140**, 2906-2918.

³ J. Zheng, R. Meana-Paneda, and D. G. Truhlar, *J. Am. Chem. Soc.*, 2014. **136**, 5150-5160.

⁴ D. G. Truhlar and Kupperma. A. *J. Am. Chem. Soc.*, 1971, **93**, 1840.

⁵ J. G. Lauderdale and D. G. Truhlar. *Surf. Sci.*, 1985, **164**, 558-588